Magnetohydrodynamics, Vol. 29, No. 2, 1993

MAGNETIC FIELD GENERATION BY AXISYMMETRIC FLOWS OF CONDUCTING LIQUIDS IN A SPHERICAL STATIONARY CONDUCTOR CAVITY

A. Gailitis

The determination of the simplest flow types capable of generating a magnetic field in a uniformly electrically conducting and incompressible medium is an important problem in the kinetic dynamo theory. Since in principle the generated field cannot be axially symmetric (Cowling's theory [1]), the axisymmetric flows, which produce an asymmetric field, are of particular interest.

Within this context, the generation conditions have been investigated previously for two schemes: for the pairs of toroidal vortices with a common axis of symmetry [2] and for the axisymmetric helical flow [3, 4]. In the first case, the velocity lies in the meridian plane and the helicity is everywhere zero. In the second, the helicity is a principal property of the flow.

Heretofore, the analysis of both schemes has been limited by the simplifying conditions. The toroidal vortices are assumed to be minute. The open helical flow is assumed to be infinitely long and to be closed across an external return zone, which is sufficiently long to make it possible to take the length effect into account using asymptotic methods [5].

In the present investigation we abandon these limitations and consider two separate problems. In both problems, the moving liquid is assumed to fill a spherical cavity in a stationary conductor. In the first problem, the motion in the cavity has the topology of two toroidal vortices, while in the second – that of a helical flow with turns and returns.

It should be noted that the first problem represents a serious computational problem requiring a fast computer with a significant memory (a RAM with a 12 MByte of a Sun Sparkstation computer was fully utilized; the computations were performed with double precision). For twenty years, our attempts to use less powerful computers were unsuccessful. Others also had tried to solve this problem [6].

Generation by means of a flow similar to that in the second scheme but situated in a cavity within an insulator has been established in [7]. We investigate the second scheme in greater detail in context with the experiment [8] using a helical sodium flow to reproduce the generation under laboratory conditions.

Problem Formulation. We consider a spherical cavity filled with a liquid having an electrical conductivity σ, which is located within a spatially infinite stationary conductor with the same conductivity. We assume that on the cavity surface a perfect electrical contact exists between the stationary and the liquid conductors. In the incompressible liquid we specify an axially symmetric motion consisting of a meridional flow with a stream function M and (in the case of the second problem) of a rotation with an angular velocity F around the symmetry axis z:

$$v_r = -(1-r^2)\frac{\partial}{\partial \cos\vartheta}(\sin^2\vartheta M(r^2, r\cos\vartheta));$$
$$v_\vartheta = -\sin\vartheta\frac{\partial}{r\partial r}(r^2(1-r^2)M(r^2, r\cos\vartheta)); \quad (1)$$
$$v_\varphi = r\sin\vartheta F(r^2, r\cos\vartheta).$$

The computing program is applicable to any arbitrary flow of an incompressible liquid, which in the spherical r, ϑ and φ coordinates is represented by closed M and F polynomials in the variables r^2 and $r\cos\vartheta$. However, in the present investigation we consider only three particular cases:

Translated from Magnitnaya Gidrodinamika, No. 2, pp. 3-14, April-June, 1993. Original article submitted February 5, 1993.

0024-998X/93/2902-0107$12.50

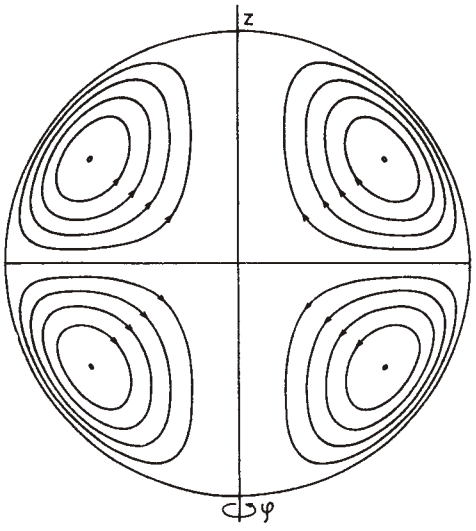

Fig. 1

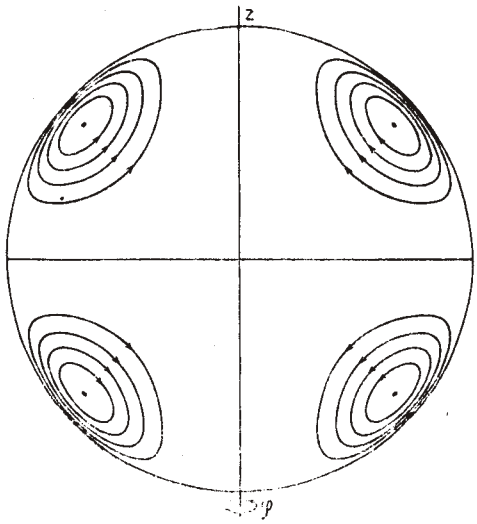

Fig. 2

Fig. 1. Flow pattern of the two contacting vortex rings model (2a).

Fig. 2. Flow pattern of the two noncontacting vortex rings model (2b).

1) M = rcosϑ, F = 0, when

$$v_r = r(1-r^2)(3\cos^2\vartheta - 1), \quad v_\vartheta = r(5r^2-3)\sin\vartheta\cos\vartheta, \quad v_\varphi = 0; \tag{2a}$$

2) $M = 4r^5\cos^3\vartheta(1-\cos^2\vartheta)$, $F = 0$, when

$$v_r = 4r^5(r^2-1)(3-10\cos^2\vartheta+7\cos^4\vartheta)\cos^2\vartheta,$$
$$v_\vartheta = 4r^5(9r^2-7)\sin^3\vartheta\cos^3\vartheta \quad v_\varphi = 0; \tag{2b}$$

3) $M = 0{,}5$, $F = 2{,}598(1-r^2)f$, when

$$v_r = (1-r^2)\cos\vartheta, \quad v_\vartheta = (2r^2-1)\sin\vartheta;$$
$$v_\varphi = 2{,}598fr(1-r^2)\sin\vartheta. \tag{2c}$$

The cavity radius R, the scale of the velocity v and the conductivity σ determine the generation only by means of the combination Rm = $\mu_0\sigma$vR, which enters directly into Eq. (3) (see further on). On this basis, the velocity scale does not enter into Eq. (1), the radius is assumed to be one (R = 1) and the so-called diffusional scale, for which $\mu_0\sigma = 1$, is used for the time.

The stream lines of the flows defined by (2a)-(2c) are shown in Figs. 1, 2, and 8. The (2a) flow represents a pair of contacting toroidal vortices, while the flow (2b) represents a pair of toroidal vortices which, however, are separated by stationary liquid both in the equatorial plane and on the axis. Topologically the flow (2c) is equivalent both to a helical flow twisted into a ring and to a helical flow enveloped by the returning flow. The coefficients in (2) are selected in such way, as to make the maximum meridional circulation velocity serve as the velocity scale and as to make the f quantity equal the maximum azimuthal velocity (see Fig. 8).

We consider only the general flow. The turbulent nature of real flows and the accompanying electromagnetic phenomena (α-effect, etc.) are not taken into account.

Method of Solution. The flow-generated field must satisfy the equation

$$\partial\mathbf{B}/\partial t = \Delta\mathbf{B} + \mathrm{Rm}\,\mathrm{rot}(\mathbf{v}\times\mathbf{B}) \tag{3}$$

and the zero condition at infinity

$$\mathbf{B}(r,\vartheta,\varphi)\to 0 \quad \text{as} \quad r\to\infty. \tag{4}$$

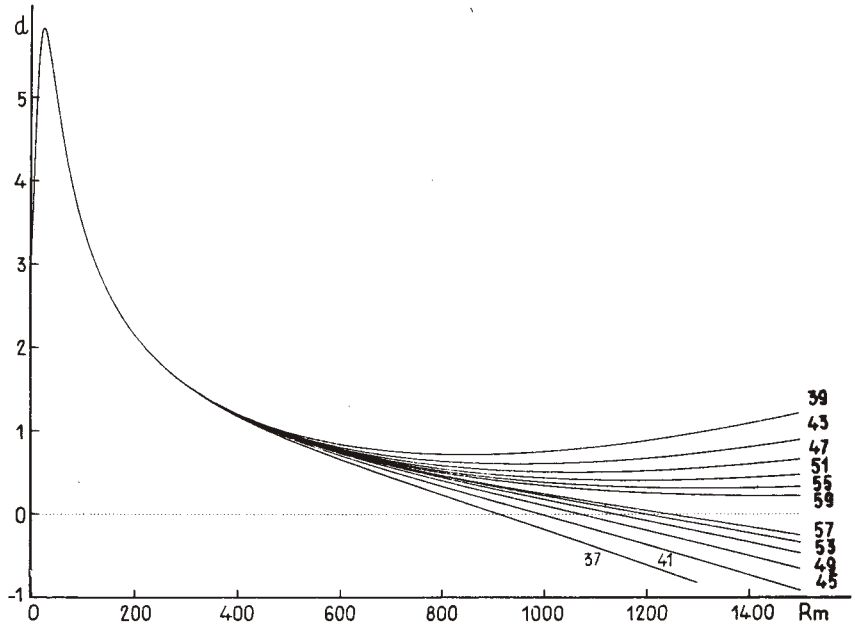

Fig. 3. Response of the model (2a) to an external excitation: the dependence of the exciting current d on the magnetic Reynolds number Rm for p = +0. l_{max} values are indicated near the curves.

A direct numerical solution of Eq. (3) is complicated by the vector nature of the **B** field. Due to div **B** = 0, only two of the three field components are independent. In the spherical coordinates, it is more convenient to use a pair a scalar functions S(r, ϑ, φ) and T(r, ϑ, φ), which express the field by the formula

$$\mathbf{B} = -i(\mathbf{r}\times\nabla T) - \mathrm{rot}(\mathbf{r}\times\nabla S), \tag{5}$$

automatically satisfying the condition div **B** = 0. In Eq. (5), the first term is called the toroidal, while the second – the poloidal field. In the dynamo problems, the substitution (5) was first used by Bullard [9] and was also presented in detail in [10]. The substitution (5) differs from that used in [10] by the factor i, which guarantees that in the cases (2a) and (2b), S and T are real. Including this factor, the equations for S and T agree with (15.42) and (15.46) described in [10].

Due to the axial symmetry and the velocity steadiness, the time and azimuth dependencies of the S and T quantities are exponential according to the exp(pt + imφ) law with m = 1, 2, 3, ... (according to the Cowling theorem, m $\neq$ 0). The p increment, which for cases (2a) and (2b) is real and complex for (2c), is determined as a computation result. The dependence of the field on r and ϑ is sought in the form of a series of adjoint Legandre functions $P_l^m(\cos\vartheta)$:

$$\begin{aligned} T(r,\vartheta,\varphi) &= \exp(im\varphi+pt)\sum_{l=m}^{\infty} t_l(r)r^l P_l^m(\cos\vartheta), \\ S(r,\vartheta,\varphi) &= \exp(im\varphi+pt)\sum_{l=m}^{\infty} s_l(r)r^l P_l^m(\cos\vartheta). \end{aligned} \tag{6}$$

The r^l factor ensures the disappearance of the derivatives of the s_l and t_l functions at zero (r = 0): $s'_l(0) = ds_l/dr \mid_{r=0} = 0$, $t'_l(0) = dt_l/dr \mid_{r=0} = 0$. The radial $s_l(r)$ and $t_l(r)$ functions are determined by numerical integration of the equations obtained by substituting (6) and (1) into (3):

$$s''_l = ps_l - 2(l+1)s'_l/r - \mathrm{Rm}\sum_{j=m}^{\infty}(U_s^{lj}s_j + U_{s'}^{lj}s'_j + U_t^{lj}t_j),$$

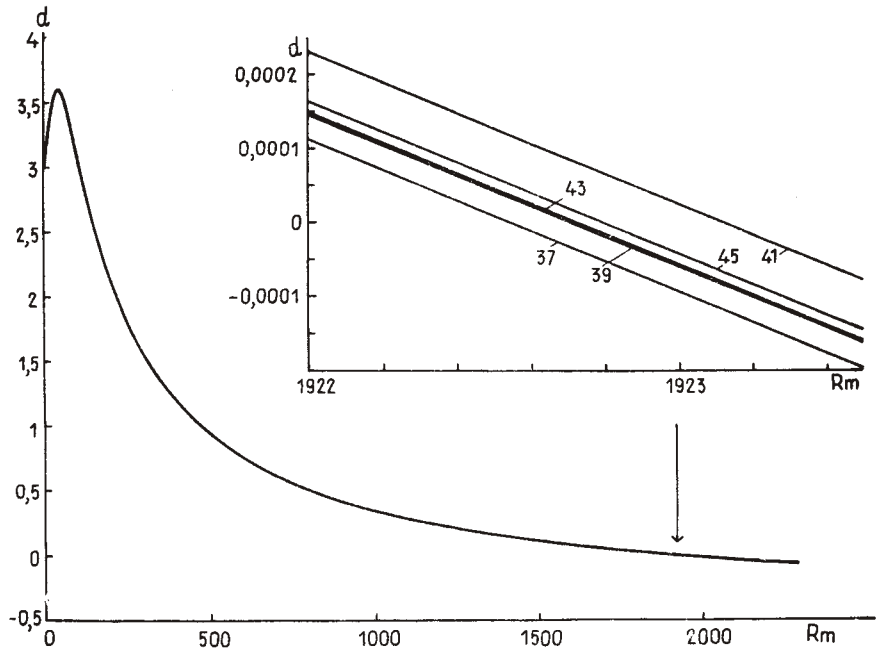

Fig. 4. The response as in Fig. 3, only for the model (2b).

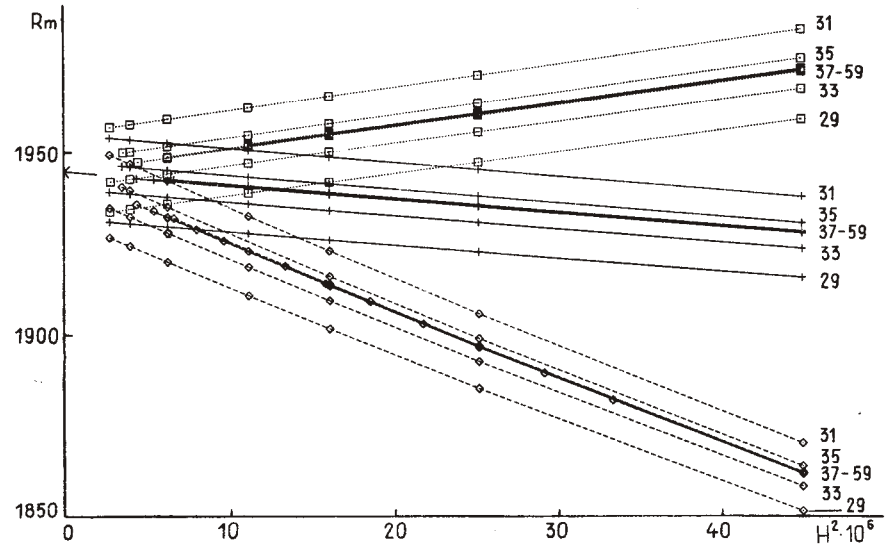

Fig. 5. Graphical correction of the critical Rm for a dipole-type field. In the lower data group from r = 0 to 1 the nodes are uniformly distributed. In the middle data group, 2/3 of the nodes are uniformly distributed between r = 0 and 0.9, with the remainder being uniformly distributed between 0.9 and 1. In the upper data group, 2/3 of the nodes are uniformly distributed between 0 and 0.9, while the remainder geometrically converge to r = 1. The corresponding $l_{\max}$ are indicated next to the curves.

$$t''_l = pt_l - 2(l+1)t'_l/r - \mathrm{Rm}\sum_{j=m}^{\infty}(V_s^{lj}s_j + V_{s'}^{lj}s'_j + V_{s''}^{lj}s''_j + V_t^{lj}t_j + V_{t'}^{lj}t'_j). \tag{7}$$

In the computations, the threshold of the self-excitation Rm is found to be a large number, and Eq. (7) belongs to a type of precipitous equations with "a small coefficient for the leading derivative." The term with s″ in the second equation is particularly troublesome: if s″ is expressed by the right hand portion of the first equation, terms appear which have an Rm^2 factor. This creates many problems in the computation.

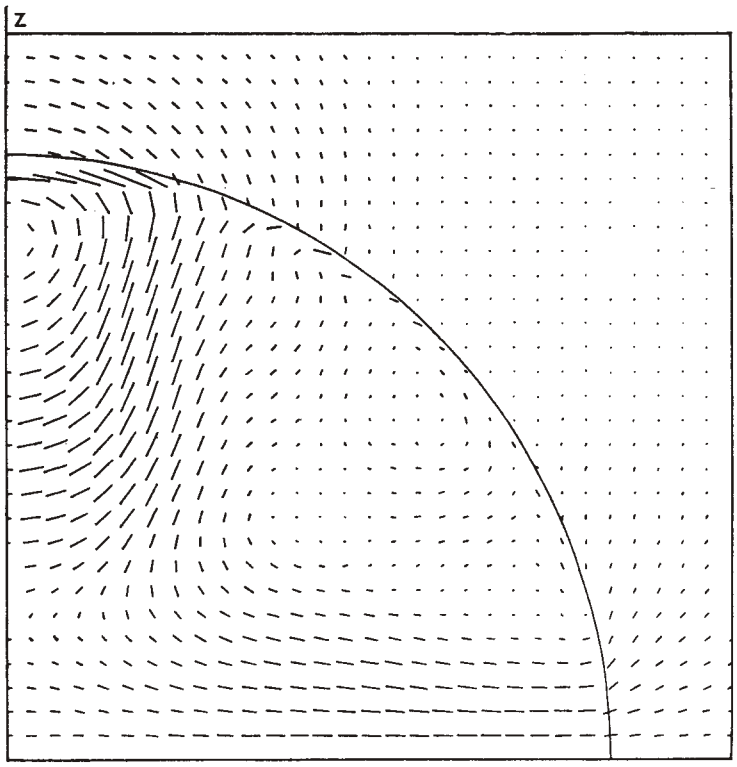

Fig. 6. Pattern of the meridional magnetic field components. The direction and numerical field magnitude correspond to the direction and length of the line segments.

The discontinuity in the tangential velocity on the spherical cavity surface makes the V_s^{lj} quantity singular and forms an inflection point (discontinuity in the derivative) of t_l at the r = 1 point:

$$\delta t'_l(1) = \mathrm{Rm} \sum_{j=m}^{\infty} D_s^{lj} s_j(1). \tag{8}$$

We shall not present the cumbersome expressions for U, V and D. The computing program forms these expressions for the chosen velocity (1) using the relations between $(d/dc)P_l^m(c)$, $cP_l^m(c)$ and $P_l^m(c)$. Inside the cavity, U and V are polynomials in r. The order of the polynomials and the maximum $l - j$ difference of the nonzero U^{lj}, U^{lj} increases if the M and F polynomials are more complicated.

Computation Methods. In the stationary (external) conductor, all $U^{lj} = V^{lj} = 0$ and the t_l and s_l are expressed in terms of modified spherical Bessel functions:

$$s_l = C_l r^{-l-1/2} K_{l+1/2}(p^{1/2} r), \qquad t_l = D_l r^{-l-1/2} K_{l+1/2}(p^{1/2} r). \tag{9}$$

The choice of the K function is specified by the condition (4).

In the moving conductor, the problem does not have an analytical solution, and the system (7) has to be integrated numerically while terminating the infinite summation at some maximum $j = l_{max}$.

The objective of the calculation is to select for each m and Rm pair (in the 2c case, a complex) a p, for which the s_l functions that are regular at zero (r = 0), are smooth for r = 1, while t_l pass to the exterior solution (9) in accordance with the conditions (8). The ultimate objective is to establish a Rm region, where increasing solutions, i.e., where Re(p) > 0, exist. Once the series are terminated, in principle, the problem can be solved using standard methods of eigenvalue calculations. However, for an indequate l_{max}, there exist also fictitious roots which do not tend towards a particular limit as the l_{max} cut-off parameter is increased; it is therefore more convenient to reformulate the problem and instead of zero in one of the smoothness conditions at r = 1, to write an auxiliary d(Rm, p) quantity, ascertaining in it the convergence with increasing l_{max} and only afterwards numerically seek p(Rm) as the root of the equation d(Rm, p) = 0.

The solutions, for which $s_m \neq 0$, are normalized by the condition $s_m(0) = 1$, while the smoothness condition is written in the form

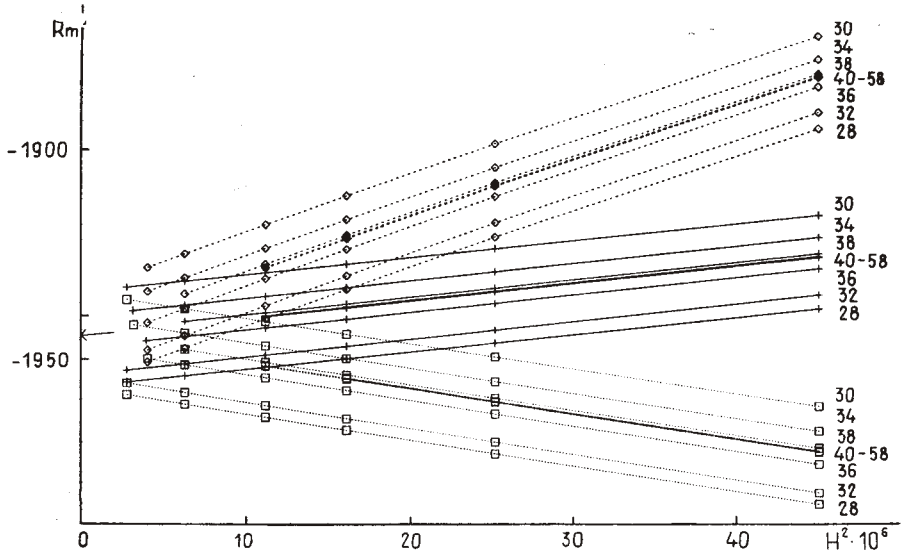

Fig. 7. Graphical correction of the critical Rm values for a quadrupole type field. The notation is the same as in Fig. 5.

$$s'_l(1-0)-s'_l(1+0)=\delta_{ml}d(\mathrm{Rm},p). \tag{10}$$

The solutions, whose symmetry ensures that $s_m = 0$ everywhere, are normalized by the condition $t_m(0) = 1$, while $\delta_{ml}d(\mathrm{Rm}, p)$ is added to the equation (8).

The d(Rm, p) quantity has the magnitude of an electric current which must be passed at r = 1 through a correspondingly wound coil in order to excite a normalized field at the cavity center; therefore, the existence of this quantity up to the generation limit, and at the limit itself, does not raise any doubts. For some Rm values, the $s_m(0)$ quantity (or $t_m(0)$) may pass through zero, and d(Rm, p) across ∞. At the generation limit (i.e., self-excitation), external excitation is unnecessary and d(Rm, p) = 0.

The introduction of d(Rm, p) results only in an insignificant increase in the computation time, since its evaluation requires solving a linear boundary value problem, i.e., Eq. (7) with the boundary conditions at two points $-s'(0) = t'(0) = 0$ for r = 0 and a matching with the exterior solutions (9) at r = 1 as outlined above. For the numerical solution, use was made of both solution methods for the two-point problems which in [11] were called the "adjustment" and "relaxation" methods.

The "adjustment" method is simpler to program and is faster in computation; it also requires less computer memory. A meeting point is selected between r = 0 and r = 1. From both ends (i.e., both from zero and from unity) to the meeting point, the (7) system is integrated by the Runge–Kutta method as many times as required for the linearly independent solutions to be consistent with the boundary conditions at the given end. After the formation of all linearly independent solutions, the system of linear algebraic equations is solved and the initial conditions at r = 0 and r = 1 are established for obtaining a smooth solution at the meeting point. This solution is found by integrating from both ends, while calculating the discrepancies and correcting the initial values until the solution becomes indeed smooth and the computed d(Rm, p) ceases to change.

Regretfully, the method is stable only up to a certain Rm value, for which a perturbation appears near the meeting point on the $s_l(r)$, $t_l(r)$ curves with a maximum l. As the Rm quantity increases, the perturbation starts at smaller l. Once the Rm value is increased by some percent, the accuracy of calculating d(Rm, p) reduces so much that the significant digits literally disappear. Using the "adjustment" method it was possible to successfully investigate only the flow (2c) and by selecting the meeting point location, to shift the instability beyond the limits of Fig. 9 (see below). For the (2a) and (2b) flows, the instability of the algorithm sets in before the appearance of field generation. The d(Rm, p) values calculated in the stable region agree with those obtained by the "relaxation" method.

In the "relaxation" method, the system (7) is approximated by difference equations, and the boundary value problem is reduced to the solution of an enormous system of linear algebraic equations. Even though the algorithm utilizes the memory extremely economically, the available number of nodes and the l_{max} values are limited by the available memory for

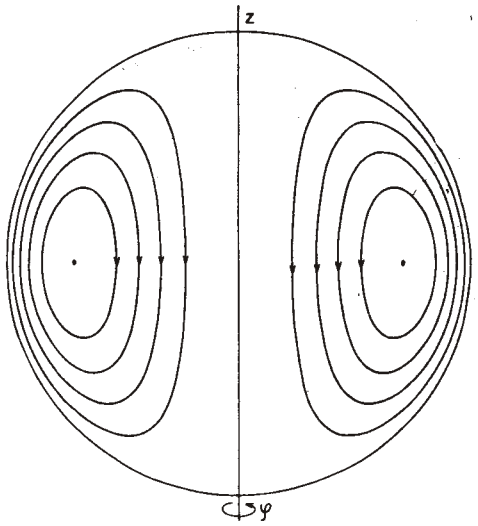

Fig. 8. Model of the short helical dynamo (2c). The meridional flow lines are simultaneously constant angular momentum density lines in the azimuthal flow.

storing the required intermediate values. The "relaxation" method was programmed by us without using complex numbers and therefore is not applicable to the flow (2c). No difficulties were encountered with the stability of the algorithm.

Computation Results for Models (2a) and (2b). Both these flows represent a pair of toroidal vortices without any azimuthal motion. The flow lines lie in the meridional plane and are shown in Fig. 1 and 2. The vortices in (2a) are thick; they involve into the flow both the equatorial plane and the axis. The vortices of (2b) are thin and are separated by stationary liquid near the equator and the axis. The behavior of both models subjected to the effect of an external excitation is shown in Fig. 3 and 4.

The conductor motion acts on the magnetic field in two ways: the field is pushed out from the region of motion and is also strengthened. Both effects are governed by a single Rm parameter and take place simultaneously. The ability of a given flow to generate a magnetic field depends on the competition between these two effects [12].

This competition is explained by Figs. 3 and 4. At small Rm values, the field displacement predominates; to maintain a normalized field, a stronger excitation is required, and the d value is increased. When the "inconvenient" field is essentially pushed out, the d value reaches a maximum. From there on, the intensification predominates and d is reduced both in Fig. 3 and in Fig. 4.

With that, the similarity of models (2a) and (2b) ends. In Fig. 3, with increasing l_{max} the d value converges so slowly as to make it impossible to find out whether or not the limiting curve intersects the axis. Thus, the question as to the capability of the flow (2a) to generate a magnetic field still remains open.

Another matter is the process depicted in Fig. 4. Here, the curves with different l_{max} values are so close to each other that even when the axis is intersected, a thousand-fold magnification is required to plot the curves individually (see the fragment in Fig. 4).

From the curves presented in Fig. 4 one can form an opinion about the smallness of the cut-off error. However, the "relaxation" method in the form employed by us is based on a second order approximation and the approximation error (in other words, the integration error) is somewhat larger than the cut-off error. The computer memory does not permit to improve the approximation by a simple increase in the node number (we used 300).

To eliminate the approximation error by means of graphic extrapolation, the critical Rm were evaluated for various l_{max} values and with different node numbers. They are all presented in Fig. 5 as a function of the squared mean arithmetic distance H between the nodes. The lower, middle and upper data groupings differ by the radial node distribution laws. In each group, the l_{max} = const lines are straight, as they should be in a second order approximation. The extensions of the central lines of all three groups intersect the Rm axis at Rm = 1944.8. This is the most plausible estimate of the critical Rm.

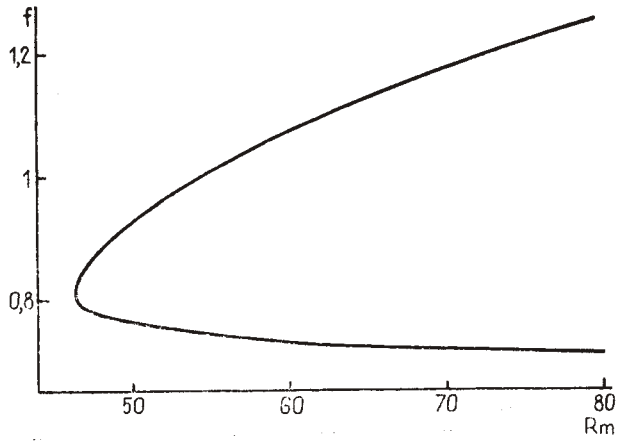

Fig. 9. Generation threshold of the helical dynamo (2c).

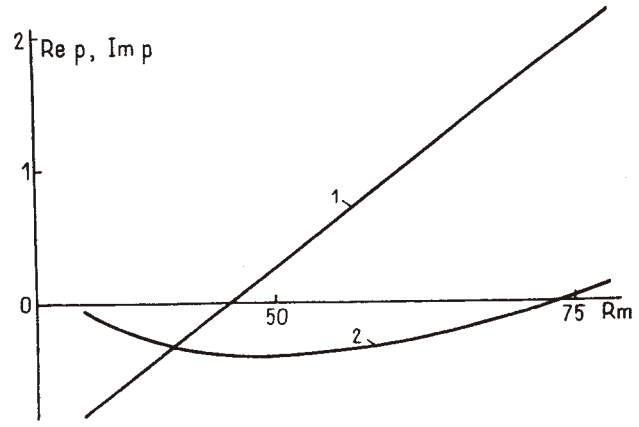

Fig. 10. Increment (1) and the generation frequency (2) of the helical dynamo (2c) for f = 0.98.

The given solution was found for m = 1 and was normalized by the condition $s_l(0) = 1$. The magnetic field pattern is presented in Fig. 6. Far off the center, the field approaches the field of a dipole perpendicular to the flow axis of symmetry. No differences were detected by comparing the field patterns calculated for various l_{max} values. By comparing the plots of the radial $s_l(r)$ and $t_l(r)$ functions, a complete conformity of the lower functions was found within the computer plotting accuracy limits. The effect of l_{max} was manifest for some higher functions, amounting to $\approx 10^{-5}$ of the lower.

No generation regions were detected for the other m values. However, for m = 1, a second generation region was found, where a quadrupole type field is produced with a leading $t_l(r)$ function. To correct the critical Rm value, Fig. 7 was plotted analogously to Fig. 5, and a 1944.8 value was obtained again but with a minus sign. The coincidence is explained by the Proctor's theorem [13, 14], which proves that in a uniformly electrically conducting medium, the flows with a specified symmetry generate fields with opposite parity but with the same magnitude and with oppositely directed velocities.

Thus, it can be assumed that the 1944.8 number was obtained by extrapolating the six independent data sets to a zero integration step, and (2b) can be recognized as a purely meridional, axially symmetric flow generating a non-axisymmetric magnetic field.

The found critical value seems to be numerically large. A number that is comparable to it is produced if in the formulae of fine vortices [2], as the small vortex radius one substitutes the distance measured in Fig. 2 from the center of the vortex rotation to the stationary conductor. A calculation in a compressible medium yields a significantly smaller number [15].

It must be noted that in Fig. 5, the cut-off parameters are only odd, while in Fig. 7 they are only even. In both cases the s-function is the highest function taken into account. Its second derivative is determined from the first of the equations (7) and with the Rm coefficient, which is a large number, enters the right hand side of the second. Neglecting it disturbs the convergence at large Rm. In the employed cut-off method such disturbance did not occur.

Results of the (2c) Model Computations. The (2c) flow represents a sum of a meridional circulation and a nonuniform rotation around the axis of symmetry. The meridional circulation lines are shown in Fig. 8. These lines are also density level lines of the angular momentum of the azimuthal flow. The Rm number is defined by the velocity of the meridional circulation at the cavity canter, where it has a maximum. The f quantity is the ratio of the maximum azimuthal velocity to the velocity at the center.

After checking various variants in the f−Rm plane, a region was found, where a rotating dipole type (m = 1) field is induced. The neutral curve is presented in Fig. 9. Inside it, the magnetic perturbations increase and on the outside they attenuate. For f = 0.98 we calculated the frequency and field increment (Fig. 10). At the threshold, the frequency is negative, meaning that the field rotates in the direction opposite to that of the liquid rotation. The computation accuracy is estimated to be 1/4 of the line thickness on the right hand side in Fig. 9 and 1/200 of the lines on the left.

What is noteworthy is the narrowness of the neutral loop and its asymmetry − for a rotation at a speed that is less than the optimum, the generation ceases abruptly, for stronger rotation, the Rm required for generation increases gradually. It must be taken into account when comparing with the calculations of the limited length helical dynamo that in [5] the Rm is referred to the internal radius, while in our investigation − to the external; therefore, the critical Rm 46 value computed here corresponds approximately to the value, which according to [5], can be expected for a short model.

It must be noted that the critical Rm value for the (2b) and (2c) models differ by a factor of 42. This indicates that the helicity is an extremely favorable, although not an indispensable factor in the dynamo process.

The computation of the (2b) model was performed at the Isaac Newton Mathematical Research Institute at Cambridge University (England) within the framework of the "Dynamo Program". The author is grateful to the Institute for its hospitality and for making the computer available.

REFERENCES

1. T. G. Cowling, "The magnetic field of sunspots," Mon. Not. R. Astron. Soc., **94,** 39-48 (1934).
2. A. Gailitis, "Self-excitation of a magnetic field by a pair of ring vortices," Magn. Gidrodin., No. 1, 39-48 (1970).
3. Yu. B. Ponomarenko, "Hydromagnetic dynamo theory," Prikl. Mekh. Tekh. Fiz., **6,** 47-51 (1973).
4. A. Gailitis and Ya. K. Freiberg, "Helical MHD dynamo theory," Magn. Gidrodin., No. 2, 3-6 (1976).
5. A. Gailitis, "The helical MHD dynamo," in: Topological Fluid Mechanics. Proc. IUTAM Symp., Cambridge, Aug. 13-18 1989, H. K. Moffatt and A. Tsinober (eds.), Cambridge, CUP (1990), pp. 147-156.
6. A. Brandenburg, private communication.
7. M. L. Dudley and R. W. James, "Time dependent kinematic dynamos with stationary flow," Proc. R. Soc. London, **A425,** 407-429 (1989).
8. A. K. Gailitis, B. G. Karasev, I. R. Kirillov, O. A. Lielausis, S. M. Luzhanskii, A. P. Ogorodnikov and G. V. Preslitskii, "An experiment with a liquid metal MHD dynamo model," Magn. Gidrodin., No. 4, 3-7 (1987).
9. E. S. Bullard and H. Gellman, "Homogeneous dynamos and terrestrial magnetism," Phil. Trans. R. Soc., **A247,** 213-378 (1954).
10. F. Krause and K.-H. Raedler, Mean-Field Magnetohydrodynamics and Dynamo Theory, Akad. Verlag, Berlin (1980).
11. W. H. Press, B. P. Flannery, S. A. Teukolsky and W. T. Vetterling, Numerical Recipes, CUP, Cambridge (1986).
12. A. Gailitis, "Magnetic field excitation by a system of submerged jets," Magn. Gidrodin., No. 3, 31-37 (1969).
13. M. R. E. Proctor, "On the eigenvalues of kinematic α-effect dynamos," Astr. Nachr., **298,** 19-25 (1977).
14. M. R. E. Proctor, "The role of mean circulation in parity selection by planetary magnetic fields," Geophys. Astrophys. Fluid Dyn., **8,** 311-324 (1977).
15. D. Moss, "A Gailitis-type dynamo in the magnetic CP stars?" Mon. Not. R. Astron. Soc., **243,** 537-542 (1990).